

# Driven and undriven states of multicomponent granular gases of inelastic and rough hard disks or spheres

Alberto Megías · Andrés Santos

February 1, 2019

**Abstract** Starting from a recent derivation of the energy production rates in terms of the number of translational and rotational degrees of freedom, a comparative study on different granular temperatures in gas mixtures of inelastic and rough disks or spheres is carried out. Both the homogeneous freely cooling state and the state driven by a stochastic thermostat are considered. It is found that the relaxation number of collisions per particle is generally smaller for disks than for spheres, the mean angular velocity relaxing more rapidly than the temperature ratios. In the asymptotic regime of the undriven system, the rotational-translational nonequipartition is stronger in disks than for spheres, while it is hardly dependent on the class of particles in the driven system. On the other hand, the degree of component-component nonequipartition is higher for spheres than for disks, both for driven and undriven systems. A study of the mimicry effect (whereby a multicomponent gas mimics the rotational-translational temperature ratio of a monocomponent gas) is also undertaken.

**Keywords** Inelastic and rough particles · Hard disks · Hard spheres · Homogeneous cooling state · Stochastic thermostat

## 1 Introduction

This paper is dedicated to the memory of Robert P. Behringer, who paved the way for a better understanding of dense granular matter. His long lasting influence and impact on the field can be appreciated in part from an excellent (posthumous) review paper [2].

While the basic model of a granular gas is a collection of inelastic and *smooth* hard disks or spheres, either monodis-

perse [3, 7, 13] or polydisperse [1, 6, 8, 9, 10, 11, 16, 25, 33, 34], the model can be significantly improved by incorporating the rotational degrees of freedom of the particles (assumed to be *rough*) [4, 5, 12, 14, 15, 17, 18, 19, 20, 21, 22, 24, 27, 31, 32, 35, 36, 37, 39]. The aim of this paper is to employ kinetic-theory methods to compare the degrees of breakdown of energy equipartition in hard disks and spheres when both roughness and polydispersity are considered. Due to the angular motion inherent to roughness, the distinction between disks and spheres is not trivial. While spinning disks on a plane have  $d_{\text{tr}} = 2$  translational and  $d_{\text{rot}} = 1$  rotational degrees of freedom, spinning spheres in space have  $d_{\text{tr}} = 3$  translational plus  $d_{\text{rot}} = 3$  rotational degrees of freedom.

In a recent work [23], we have presented a *unified* kinetic-theory derivation (in terms of the number of degrees of freedom  $d_{\text{tr}}$  and  $d_{\text{rot}}$ ) of the collisional rates of energy production in multicomponent granular gases, so that previous results for disks [29] and spheres [30] are obtained by taking  $(d_{\text{tr}}, d_{\text{rot}}) = (2, 1)$  and  $(d_{\text{tr}}, d_{\text{rot}}) = (3, 3)$ , respectively. Those unified expressions will be applied here to study the granular temperature ratios in monodisperse and bidisperse gases of rough disks or spheres in homogeneous states, both undriven and driven.

The remainder of the paper is organized as follows. Section 2 defines the systems and presents the energy production rates. This is followed by the application to the homogeneous cooling state (HCS) and to the state driven by a stochastic thermostat in Secs. 3 and 4, respectively. Section 5 deals with the conditions for a mixture to mimic a monocomponent gas in what concerns the temperature ratios (mimicry effect). Finally, the conclusions are presented in Sec. 6.

A. Megías · A. Santos  
Departamento de Física, Universidad de Extremadura, E-06006 Badajoz, Spain

## 2 Energy production rates

Let us consider a dilute multicomponent granular gas made of hard disks or spheres of different masses  $\{m_i\}$ , diameters  $\{\sigma_i\}$ , and moments of inertia  $\{I_i \equiv \kappa_i m_i \sigma_i^2/4\}$ . We denote by  $\mathbf{v}_i$  and  $\boldsymbol{\omega}_i$  the translational and angular velocities, respectively, of a particle belonging to component  $i$ . In a binary collision between particles of components  $i$  and  $j$ , linear total momentum is conserved, as is the angular momentum of each particle with respect to the point of contact, but this is not enough to determine the postcollisional velocities in terms of the precollisional ones and the unit vector  $\hat{\boldsymbol{\sigma}}$  pointing from the center of particle  $i$  to the center of particle  $j$ . To close the collision rules, it is frequently assumed that the normal and tangential components of the relative velocity  $\mathbf{w}_{ij} \equiv \mathbf{v}_i - \mathbf{v}_j - \hat{\boldsymbol{\sigma}} \times (\boldsymbol{\sigma}_i \boldsymbol{\omega}_i + \boldsymbol{\sigma}_j \boldsymbol{\omega}_j)/2$  of the points of the particles at contact become, after collision,  $\mathbf{w}'_{ij} \cdot \hat{\boldsymbol{\sigma}} = -\alpha_{ij} \mathbf{w}_{ij} \cdot \hat{\boldsymbol{\sigma}}$ ,  $\hat{\boldsymbol{\sigma}} \times \mathbf{w}'_{ij} = -\beta_{ij} \hat{\boldsymbol{\sigma}} \times \mathbf{w}_{ij}$ , where  $\alpha_{ij}$  and  $\beta_{ij}$  are the coefficients of normal and tangential restitution, respectively. The coefficient  $\alpha_{ij}$  ranges from  $\alpha_{ij} = 0$  (perfectly inelastic particles) to  $\alpha_{ij} = 1$  (perfectly elastic particles). In contrast,  $\beta_{ij}$  ranges from  $\beta_{ij} = -1$  (perfectly smooth particles) to  $\beta_{ij} = 1$  (perfectly rough particles). It can be easily checked that the total (translational plus rotational) kinetic energy is a collisional invariant only if  $\alpha_{ij} = |\beta_{ij}| = 1$ .

The mean values of the translational and rotational kinetic energies of particles of component  $i$  define the so-called (partial) *granular* temperatures, namely [30]  $T_i^{\text{tr}} = m \langle v_i^2 \rangle / d_{\text{tr}}$ ,  $T_i^{\text{rot}} = I_i \langle \omega_i^2 \rangle / d_{\text{rot}}$ , where, as said before,  $d_{\text{tr}}$  and  $d_{\text{rot}}$  are the number of translational and rotational degrees of freedom, respectively, and a zero mean translational velocity has been assumed. Analogously, one can define the mean angular velocity of component  $i$  as  $\boldsymbol{\Omega}_i = \langle \boldsymbol{\omega}_i \rangle$ . The rates of change of the quantities  $\boldsymbol{\Omega}_i$ ,  $T_i^{\text{tr}}$ , and  $T_i^{\text{rot}}$  due to collisions with particles of component  $j$  can be written as

$$\partial_t \boldsymbol{\Omega}_i |_{\text{coll},j} = -\frac{\xi_{ij}^{\Omega}}{2} \left( \boldsymbol{\Omega}_i + \frac{\boldsymbol{\sigma}_j}{\sigma_i} \boldsymbol{\Omega}_j \right), \quad (1a)$$

$$\partial_t T_i^{\text{tr}} |_{\text{coll},j} = -\xi_{ij}^{\text{tr}} T_i^{\text{tr}}, \quad \partial_t T_i^{\text{rot}} |_{\text{coll},j} = -\xi_{ij}^{\text{rot}} T_i^{\text{rot}}, \quad (1b)$$

where  $\xi_{ij}^{\Omega}$  are spin production rates, and  $\xi_{ij}^{\text{tr}}$  and  $\xi_{ij}^{\text{rot}}$  are energy production rates. While the exact determination of those quantities is not possible, a kinetic-theory approach (namely the Boltzmann equation) supplemented by a Maxwellian approximation [23, 29, 30] allows one to express them in terms of the partial densities ( $n_i$ ,  $n_j$ ), temperatures ( $T_i^{\text{tr}}$ ,  $T_i^{\text{rot}}$ ,  $T_j^{\text{tr}}$ ,  $T_j^{\text{rot}}$ ), mean angular velocities ( $\boldsymbol{\Omega}_i$ ,  $\boldsymbol{\Omega}_j$ ), and the mechanical parameters. The unified expressions for disks ( $d_{\text{tr}} = 2$ ,

$d_{\text{rot}} = 1$ ) and spheres ( $d_{\text{tr}} = d_{\text{rot}} = 3$ ) are [23]

$$\xi_{ij}^{\Omega} = \frac{v_{ij}}{d_{\text{tr}}} \frac{4m_{ij} \bar{\beta}_{ij}}{m_i \kappa_i}, \quad v_{ij} \equiv \frac{\sqrt{2\pi} \frac{d_{\text{tr}}-1}{2}}{\Gamma(d_{\text{tr}}/2)} n_j \sigma_{ij}^{d_{\text{tr}}-1} \sqrt{\frac{T_i^{\text{tr}}}{m_i} + \frac{T_j^{\text{tr}}}{m_j}}, \quad (2a)$$

$$\xi_{ij}^{\text{tr}} = \frac{v_{ij}}{d_{\text{tr}}} \frac{2m_{ij}^2}{m_i T_i^{\text{tr}}} \left[ 2 \left( \bar{\alpha}_{ij} + \frac{d_{\text{rot}}}{d_{\text{tr}}} \bar{\beta}_{ij} \right) \frac{T_i^{\text{tr}}}{m_j} - \left( \bar{\alpha}_{ij}^2 + \frac{d_{\text{rot}}}{d_{\text{tr}}} \bar{\beta}_{ij}^2 \right) \left( \frac{T_i^{\text{tr}}}{m_i} + \frac{T_j^{\text{tr}}}{m_j} \right) - \frac{d_{\text{rot}}}{d_{\text{tr}}} \bar{\beta}_{ij}^2 \left( \frac{T_i^{\text{rot}}}{m_i \kappa_i} + \frac{T_j^{\text{rot}}}{m_j \kappa_j} + \frac{\boldsymbol{\sigma}_i \boldsymbol{\sigma}_j \boldsymbol{\Omega}_i \cdot \boldsymbol{\Omega}_j}{2d_{\text{rot}}} \right) \right], \quad (2b)$$

$$\xi_{ij}^{\text{rot}} = \frac{v_{ij}}{d_{\text{tr}}} \frac{4m_{ij}^2 \bar{\beta}_{ij}}{m_i \kappa_i T_i^{\text{rot}}} \left[ \frac{T_i^{\text{rot}}}{m_j} + \frac{m_i \kappa_i}{m_j} \frac{\boldsymbol{\sigma}_i \boldsymbol{\sigma}_j \boldsymbol{\Omega}_i \cdot \boldsymbol{\Omega}_j}{4d_{\text{rot}}} - \frac{\bar{\beta}_{ij}}{2} \left( \frac{T_i^{\text{tr}}}{m_i} + \frac{T_j^{\text{tr}}}{m_j} + \frac{T_i^{\text{rot}}}{m_i \kappa_i} + \frac{T_j^{\text{rot}}}{m_j \kappa_j} + \frac{\boldsymbol{\sigma}_i \boldsymbol{\sigma}_j \boldsymbol{\Omega}_i \cdot \boldsymbol{\Omega}_j}{2d_{\text{rot}}} \right) \right]. \quad (2c)$$

Here,  $\bar{\alpha}_{ij} \equiv 1 + \alpha_{ij}$ ,  $\bar{\beta}_{ij} \equiv (1 + \beta_{ij}) \kappa_{ij} / (1 + \kappa_{ij})$ ,  $m_{ij} \equiv m_i m_j / (m_i + m_j)$ ,  $\kappa_{ij} \equiv \kappa_i \kappa_j (m_i + m_j) / (\kappa_i m_i + \kappa_j m_j)$ ,  $\boldsymbol{\sigma}_{ij} \equiv \frac{1}{2} (\boldsymbol{\sigma}_i + \boldsymbol{\sigma}_j)$ .

In the special case of a monocomponent gas, Eqs. (2) become

$$\xi^{\Omega} = \frac{2v}{d_{\text{tr}}} \frac{1 + \beta}{1 + \kappa}, \quad v \equiv \frac{2\pi \frac{d_{\text{tr}}-1}{2}}{\Gamma(d_{\text{tr}}/2)} n \sigma^{d_{\text{tr}}-1} \sqrt{\frac{T^{\text{tr}}}{m}}, \quad (3a)$$

$$\xi^{\text{tr}} = \frac{v}{d_{\text{tr}}} \left\{ 1 - \alpha^2 + \frac{2d_{\text{rot}} \kappa (1 + \beta)}{d_{\text{tr}} (1 + \kappa)^2 T^{\text{tr}}} \left[ \frac{\kappa (1 - \beta)}{2} \left( T^{\text{tr}} + \frac{T^{\text{rot}}}{\kappa} + \frac{m \sigma^2 \Omega^2}{4d_{\text{rot}}} \right) + T^{\text{tr}} - T^{\text{rot}} - \frac{\kappa m \sigma^2 \Omega^2}{4d_{\text{rot}}} \right] \right\}, \quad (3b)$$

$$\xi^{\text{rot}} = \frac{2v}{d_{\text{tr}}} \frac{\kappa (1 + \beta)}{(1 + \kappa)^2 T^{\text{rot}}} \left[ \frac{1 - \beta}{2} \left( T^{\text{tr}} + \frac{T^{\text{rot}}}{\kappa} + \frac{m \sigma^2 \Omega^2}{4d_{\text{rot}}} \right) + T^{\text{rot}} - T^{\text{tr}} + \frac{\kappa m \sigma^2 \Omega^2}{4d_{\text{rot}}} \right]. \quad (3c)$$

Note that Eqs. (2) and (3) are obtained from the results of Ref. [23] with the replacement  $d_{\text{tr}} - 1 \rightarrow 2d_{\text{rot}}/d_{\text{tr}}$ , which holds for both disks and spheres.

## 3 Undriven gas: Homogeneous cooling state

In the HCS, time evolution of the mean values is due to collisions only. In particular,  $\partial_t T_i^{\text{tr}} = -\xi_i^{\text{tr}} T_i^{\text{tr}}$ ,  $\partial_t T_i^{\text{rot}} = -\xi_i^{\text{rot}} T_i^{\text{rot}}$ , where  $\xi_i^{\text{tr}} \equiv \sum_j \xi_{ij}^{\text{tr}}$  and  $\xi_i^{\text{rot}} \equiv \sum_j \xi_{ij}^{\text{rot}}$ . In the long-time asymptotic regime, all temperatures decay with a common rate, so that the temperature ratios are obtained from the conditions that the temperature ratios are constant:  $\xi_1^{\text{tr}} = \xi_2^{\text{tr}} = \dots = \xi_1^{\text{rot}} = \xi_2^{\text{rot}} = \dots$ . Our goal now is to compare those ratios in the cases of hard disks and hard spheres. To that end, we will suppose a uniform mass distribution in both types of particles, so that the reduced moment of inertia is  $\kappa_i = \frac{1}{2}$  for disks and  $\kappa_i = \frac{2}{5}$  for spheres.

### 3.1 Monocomponent system

Given the three energy scales  $T^{\text{tr}}$ ,  $T^{\text{rot}}$ , and  $I\Omega^2$  we can construct the following two dimensionless quantities:  $\theta \equiv T^{\text{rot}}/T^{\text{tr}}$  and  $X \equiv I\Omega^2/d_{\text{rot}}T^{\text{rot}} = \langle \boldsymbol{\omega} \rangle^2 / \langle \omega^2 \rangle$ . Using Eqs. (3), one can obtain in a straightforward way a coupled set of nonlinear differential equations for the evolution of  $\theta$  and  $X$ :

$$\frac{1}{2} \partial_\tau \ln \theta + \xi^{\text{rot},*} - \xi^{\text{tr},*} = \frac{1}{2} \partial_\tau \ln X + 2\xi^{\Omega,*} - \xi^{\text{rot},*} = 0, \quad (4)$$

where a star denotes division by the collision frequency  $\nu$  (i.e.,  $\xi^{\text{tr},*} \equiv \xi^{\text{tr}}/\nu$ , etc.) and  $\tau = \frac{1}{2} \int_0^t dt' \nu(t')$  is the accumulated number of collisions per particle. Taking into account that  $X < 1$ , it can be easily checked that  $2\xi^{\Omega,*} - \xi^{\text{rot},*}$  is positive definite, thus implying that  $\lim_{\tau \rightarrow \infty} X(\tau) = 0$ . On the other hand, the evolution equation for  $\theta(\tau)$  admits a stationary solution,  $\theta_s$ , given by the condition  $\xi^{\text{tr},*} = \xi^{\text{rot},*}$ , which yields a quadratic equation whose physical solution is

$$\theta_s = \sqrt{\left[ h + \frac{1}{2} \left( 1 - \frac{d_{\text{tr}}}{d_{\text{rot}}} \right) \right]^2 + \frac{d_{\text{tr}}}{d_{\text{rot}}} + h + \frac{1}{2} \left( 1 - \frac{d_{\text{tr}}}{d_{\text{rot}}} \right)}, \quad (5a)$$

$$h \equiv \frac{d_{\text{tr}}(1 + \kappa)^2}{2d_{\text{rot}}\kappa(1 + \beta)^2} \left[ 1 - \alpha^2 - \frac{1 - \frac{d_{\text{rot}}}{d_{\text{tr}}}\kappa}{1 + \kappa} (1 - \beta^2) \right]. \quad (5b)$$

Figure 1 shows a density plot of the stationary temperature ratio  $\theta_s$  as a function of the coefficients of restitution  $\alpha$  and  $\beta$  in the cases of (a) uniform disks ( $\kappa = \frac{1}{2}$ ) and (b) uniform spheres ( $\kappa = \frac{2}{5}$ ). In both cases, the equipartition line  $\theta_s = 1$  (where  $h = 0$ ) splits the plane ( $\beta, \alpha$ ) into two regions. In the lower region, the rotational temperature is higher than the translational one ( $\theta_s > 1, h > 0$ ), while the opposite occurs in the upper region. Apart from those common features, we can observe that, in general, the breakdown of rotational-translational equipartition is higher in disks than in spheres.

Once the stationary solution  $(\theta, X) = (\theta_s, 0)$  of the HCS is established, it is convenient to analyze its stability. Linearization of the evolution equations (4) yields the solution

$$\delta\theta(\tau) = \delta\theta_0 e^{-\lambda_1 \tau} - \frac{\lambda_{12}}{\lambda_2 - \lambda_1} X_0 \left( e^{-\lambda_1 \tau} - e^{-\lambda_2 \tau} \right), \quad (6a)$$

$$X(\tau) = X_0 e^{-\lambda_2 \tau}, \quad (6b)$$

where  $\delta\theta(\tau) \equiv \theta(\tau) - \theta_s$  and

$$\lambda_1 = \frac{2\kappa}{d_{\text{tr}}} \left( \frac{1 + \beta}{1 + \kappa} \right)^2 \left( \frac{1}{\theta_s} + \frac{d_{\text{rot}}}{d_{\text{tr}}} \theta_s \right), \quad (7a)$$

$$\lambda_2 = \frac{2}{d_{\text{tr}}} \frac{1 + \beta}{1 + \kappa} \left[ 2 + (1 + \beta) \frac{1 + \kappa/\theta_s}{1 + \kappa} \right], \quad (7b)$$

$$\lambda_{12} = \frac{2\theta_s}{d_{\text{tr}}} \frac{1 + \beta}{(1 + \kappa)^2} \left[ 2\kappa + 1 - \beta + \frac{d_{\text{rot}}}{d_{\text{tr}}} (1 + \beta) \kappa \theta_s \right]. \quad (7c)$$

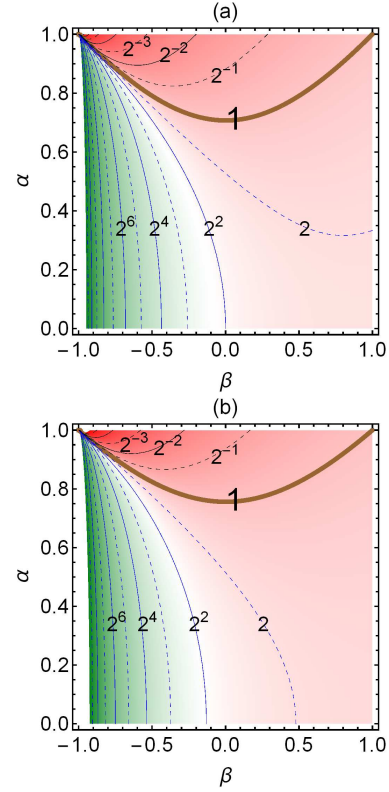


**Fig. 1** Density plot of the stationary value  $\theta_s$  of the temperature ratio  $\theta \equiv T^{\text{rot}}/T^{\text{tr}}$  in the HCS [see Eqs. (5)] for (a) uniform disks ( $\kappa = \frac{1}{2}$ ) and (b) uniform spheres ( $\kappa = \frac{2}{5}$ ). The contour lines correspond to  $\theta_s = 1$  (thick solid line),  $\theta_s = 2^{-1}, 2^{-2}, 2^{-3}, \dots$ , and  $\theta_s = 2, 2^2, 2^3, \dots$

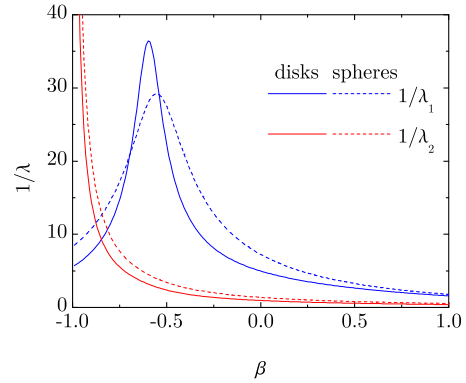


**Fig. 2** Plot of the relaxation times  $1/\lambda_1$  (blue lines) and  $1/\lambda_2$  (red lines) versus  $\beta$  at  $\alpha = 0.8$  in the HCS [see Eqs. (7)] for uniform disks (solid lines) and uniform spheres (dashed lines).

As expected on physical grounds, both eigenvalues  $\lambda_1$  and  $\lambda_2$  are positive definite, what confirms the stability of the stationary solution  $(\theta, X) = (\theta_s, 0)$  with respect to homogeneous perturbations. The quantities  $1/\lambda_1$  and  $1/\lambda_2$  are the characteristic relaxation times (measured as the number of collisions per particle) associated with the evolution of  $\delta\theta(\tau)$  (if  $X_0 = 0$  or  $\lambda_1 < \lambda_2$ ) and  $X(\tau)$ , respectively. Both

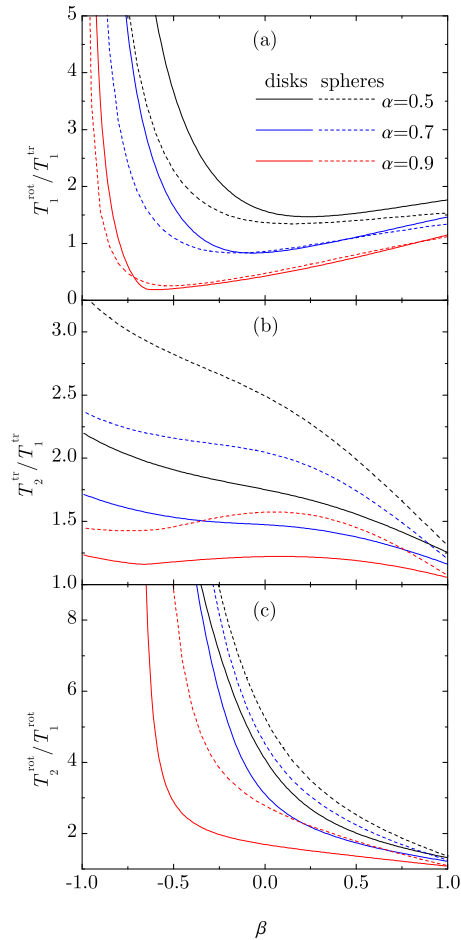


**Fig. 3** Plot of the temperature ratios (a)  $T_1^{\text{rot}}/T_1^{\text{tr}}$ , (b)  $T_2^{\text{tr}}/T_1^{\text{tr}}$ , and (c)  $T_2^{\text{rot}}/T_1^{\text{rot}}$  versus  $\beta$  in the HCS for equimolar binary mixtures of uniform disks (solid lines) or uniform spheres (dashed lines) with  $\sigma_2/\sigma_1 = 2$ ,  $m_2/m_1 = 2^{d_{\text{tr}}}$ ,  $\beta_{ij} = \beta$ , and  $\alpha_{ij} = \alpha = 0.5$  (black lines), 0.7 (blue lines), and 0.9 (red lines).

relaxation times are plotted in Fig. 2 as functions of the coefficient of tangential restitution at the representative value  $\alpha = 0.8$ . It can be observed that, except for very small roughness ( $-1 \lesssim \beta \lesssim 0.84$ ), one has  $1/\lambda_2 < 1/\lambda_1$ . This justifies the non-hydrodynamic character of the angular velocity in a hydrodynamic description [18]. As for the difference between disks and spheres, Fig. 2 also shows that, in general, disks require a smaller number of collisions than spheres to reach the stationary state. The only exception is the interval  $-0.69 \lesssim \beta \lesssim -0.54$ , where  $1/\lambda_1$  is larger for disks than for spheres.

### 3.2 Binary system

As a representative multicomponent gas, let us consider here a binary system that has already reached the asymptotic HCS. The conditions  $\xi_1^{\text{tr}} = \xi_1^{\text{rot}} = \xi_2^{\text{tr}} = \xi_2^{\text{rot}}$  provide the three independent temperature ratios ( $T_1^{\text{rot}}/T_1^{\text{tr}}$ ,  $T_2^{\text{tr}}/T_1^{\text{tr}}$ , and  $T_2^{\text{rot}}/T_1^{\text{rot}}$ )

for arbitrary values of the 11 dimensionless parameters of the system ( $n_2/n_1$ ,  $m_2/m_1$ ,  $\sigma_2/\sigma_1$ ,  $\kappa_1$ ,  $\kappa_2$ ,  $\alpha_{11}$ ,  $\alpha_{12}$ ,  $\alpha_{22}$ ,  $\beta_{11}$ ,  $\beta_{12}$ , and  $\beta_{22}$ ). For the sake of concreteness, we will consider an equimolar mixture ( $n_2/n_1 = 1$ ) where all the particles are uniform ( $\kappa_i = \frac{1}{2}$  and  $\frac{2}{5}$  for disks and spheres, respectively) and made of the same material (i.e.,  $\alpha_{ij} = \alpha$  and  $\beta_{ij} = \beta$ ). Moreover, the size of the large particles is assumed to be twice that of the small particles ( $\sigma_2/\sigma_1 = 2$ ), so that  $m_2/m_1 = 2^{d_{\text{tr}}}$ .

Figure 3 shows the three independent temperature ratios as functions of the roughness parameter  $\beta$  for a few characteristic values of the inelasticity parameter  $\alpha$ . The rotational-translational temperature ratios  $T_1^{\text{rot}}/T_1^{\text{tr}}$  have a behavior qualitatively similar to that of the monodisperse case (see Fig. 1) in the sense that  $T_1^{\text{rot}}/T_1^{\text{tr}} < 1$  if  $\alpha$  is larger than a certain threshold value and  $\beta$  belongs to a certain  $\alpha$ -dependent interval around  $\beta \approx 0$ , whereas  $T_1^{\text{rot}}/T_1^{\text{tr}} > 1$  otherwise. Also, the departure from rotational-translational equipartition ( $T_1^{\text{rot}}/T_1^{\text{tr}} = 1$ ) is generally stronger for disks than for spheres. In contrast, Figs. 3(b) and 3(c) show that the translational and rotational component-component ratios exhibit a stronger nonequipartition effect in the case of spheres than in the case of disks.

## 4 Driven gas: Stochastic thermostat

Let us consider now a homogeneous dilute granular gas subject to a stochastic volume force  $\mathbf{F}^{\text{wn}}$  (also called a thermostat), which injects translational kinetic energy to the particles and has the properties of a Gaussian white noise [1, 26, 28, 38], i.e.,  $\langle \mathbf{F}_i^{\text{wn}}(t) \rangle = \mathbf{0}$ ,  $\langle \mathbf{F}_i^{\text{wn}}(t) \mathbf{F}_j^{\text{wn}}(t') \rangle = l m_i^2 \chi_0^2 \delta_{ij} \delta(t - t')$ , where indices  $i, j$  refer to particles,  $l$  is the  $d_{\text{tr}} \times d_{\text{tr}}$  unit matrix, and  $\chi_0^2$  measures the strength of the stochastic force. This kind of forcing can model, for example, the energy input to grains immersed in a gas in turbulent flow.

Since the stochastic force acts on the translational degrees of freedom only, the time evolutions of the mean angular velocities ( $\langle \boldsymbol{\Omega}_i \rangle$ ) and the rotational temperatures ( $T_i^{\text{rot}}$ ) are governed by collisions only. On the other hand,  $\partial_t T_i^{\text{tr}} = m_i \chi_0^2 - \xi_i^{\text{tr}} T_i^{\text{tr}}$ . The conditions for a stationary state are  $\langle \boldsymbol{\Omega}_i \rangle = \mathbf{0}$ ,  $\xi_i^{\text{rot}} = 0$ , and  $m_i \chi_0^2 = \xi_i^{\text{tr}} T_i^{\text{tr}}$ .

### 4.1 Monocomponent system

Apart from  $X \equiv I\Omega^2/d_{\text{rot}}T^{\text{rot}}$  and  $\theta \equiv T^{\text{rot}}/T^{\text{tr}}$ , the stochastic thermostat introduces a third dimensionless parameter,  $Y \equiv m\chi_0^2/vT^{\text{tr}}$ , which can be seen as a (time-dependent) reduced measure of the noise strength. Instead of Eq. (4), now

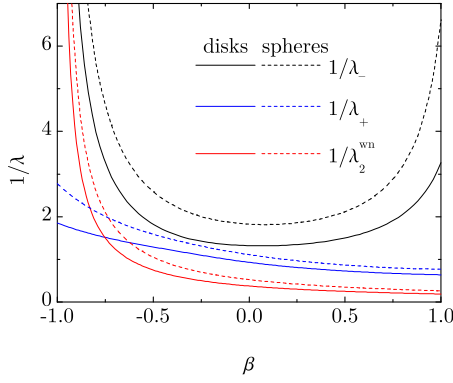


**Fig. 4** Plot of the relaxation times  $1/\lambda_-$  (black lines),  $1/\lambda_+$  (blue lines), and  $1/\lambda_2^{\text{wn}}$  (red lines) versus  $\beta$  at  $\alpha = 0.8$  in systems driven by a stochastic thermostat [see Eqs. (11)] for uniform disks (solid lines) and uniform spheres (dashed lines).

we have

$$\begin{aligned} \frac{1}{2} \partial_\tau \ln \theta + \xi^{\text{rot},*} - \xi^{\text{tr},*} + Y &= \frac{1}{2} \partial_\tau \ln X + 2\zeta^{\Omega,*} - \xi^{\text{rot},*} \\ &= \frac{1}{2} \partial_\tau \ln Y + \frac{3}{2} (Y - \xi^{\text{tr},*}) = 0. \end{aligned} \quad (8)$$

As in the undriven case,  $2\zeta^{\Omega,*} - \xi^{\text{rot},*}$  is positive definite, so that  $\lim_{\tau \rightarrow \infty} X(\tau) = 0$ . Moreover,  $\xi^{\text{rot},*} = 0$  and  $Y - \xi^{\text{tr},*} = 0$  give the stationary values

$$\theta_s^{\text{wn}} = \frac{1 + \beta}{2 + \kappa^{-1}(1 - \beta)}, \quad Y_s = \frac{1 - \alpha^2}{d_{\text{tr}}} + \frac{2d_{\text{rot}}}{d_{\text{tr}}^2} (1 - \beta) \theta_s^{\text{wn}}. \quad (9)$$

Note that  $\theta_s^{\text{wn}}$  is independent of  $\alpha$ ,  $d_{\text{tr}}$ , and  $d_{\text{rot}}$ . However, it depends on the reduced moment of inertia  $\kappa$ , so that it is slightly larger for uniform disks ( $\kappa = \frac{1}{2}$ ) than for uniform spheres ( $\kappa = \frac{2}{5}$ ). Since  $\theta_s^{\text{wn}} \leq 1$ , this implies that, in contrast to the HCS case, the degree of rotational-translational nonequipartition is higher in spheres than in disks.

As in the HCS case, it is instructive to analyze the time evolution of  $\delta\theta \equiv \theta - \theta_s^{\text{wn}}$ ,  $\delta Y \equiv Y - Y_s$  and  $X$  near the stationary state. After linearizing Eqs. (8), one obtains

$$\delta\theta(\tau) + \frac{\lambda_\pm - \lambda_1^{\text{wn}}}{\lambda_{31}} \delta Y(\tau) = \left( \delta\theta_0 + \frac{\lambda_\pm - \lambda_1^{\text{wn}}}{\lambda_{31}} \delta Y_0 \right) e^{-\lambda_\pm \tau} - \frac{\lambda_\pm \theta_s^{\text{wn}} X_0}{\lambda_2^{\text{wn}} - \lambda_\pm} \left( e^{-\lambda_\pm \tau} - e^{-\lambda_2^{\text{wn}} \tau} \right), \quad (10a)$$

$$X(\tau) = X_0 e^{-\lambda_2^{\text{wn}} \tau}, \quad (10b)$$

where

$$\lambda_\pm = \frac{1}{2} \left[ \lambda_1^{\text{wn}} + 3Y_s \pm \sqrt{(\lambda_1^{\text{wn}} - 3Y_s)^2 + 8\theta_s^{\text{wn}} \lambda_{31}} \right], \quad (11a)$$

$$\lambda_1^{\text{wn}} = \frac{2\kappa}{d_{\text{tr}}} \left( \frac{1 + \beta}{1 + \kappa} \right)^2 \left( \frac{1}{\theta_s^{\text{wn}}} + \frac{d_{\text{rot}}}{d_{\text{tr}}} \theta_s^{\text{wn}} \right), \quad (11b)$$

$$\lambda_2^{\text{wn}} = \frac{8}{d_{\text{tr}}} \frac{1 + \beta}{1 + \kappa}, \quad \lambda_{31} = \frac{3d_{\text{rot}} \kappa}{d_{\text{tr}}^2} \left( \frac{1 + \beta}{1 + \kappa} \right)^2 Y_s. \quad (11c)$$

The dependence on  $\beta$  of the reciprocal eigenvalues  $1/\lambda_\pm$  and  $1/\lambda_2^{\text{wn}}$  is shown in Fig. 4 at  $\alpha = 0.8$ . Comparison with Fig. 2 shows that the relaxation toward the stationary values is much faster in the driven gas than in the undriven one. Although  $1/\lambda_+ < 1/\lambda_2^{\text{wn}}$  if  $\beta \lesssim -0.74$ , one has  $1/\lambda_- > 1/\lambda_2^{\text{wn}}$  for all  $\beta$ , so that the reduced angular velocity  $X$  tends to zero much more rapidly than  $\delta\theta$  and  $\delta Y$ . Finally, in agreement with the undriven case, we can observe that the relaxation times (as measured by the number of collisions per particle) are shorter for disks than for spheres.

## 4.2 Binary system

In the case of a binary mixture driven by a stochastic thermostat, the three independent temperature ratios ( $T_1^{\text{rot}}/T_1^{\text{tr}}$ ,  $T_2^{\text{tr}}/T_1^{\text{tr}}$ , and  $T_2^{\text{rot}}/T_1^{\text{rot}}$ ) in the steady state are obtained by the conditions  $\xi_1^{\text{rot}} = \xi_2^{\text{rot}} = 0$  and  $\xi_1^{\text{tr}} T_1^{\text{tr}}/m_1 = \xi_2^{\text{tr}} T_2^{\text{tr}}/m_2$ . Again, we choose here an equimolar mixture ( $n_2/n_1 = 1$ ) with  $\kappa_i = \frac{1}{2}$  and  $\frac{2}{5}$  for disks and spheres, respectively,  $\alpha_{ij} = \alpha$ ,  $\beta_{ij} = \beta$ ,  $\sigma_2/\sigma_1 = 2$ , and  $m_2/m_1 = 2^{d_{\text{tr}}}$ .

The temperature ratios are shown in Fig. 5 as functions of the roughness parameter  $\beta$  for the same values of  $\alpha$  as in Fig. 3. The rotational-translational temperature ratio  $T_1^{\text{rot}}/T_1^{\text{tr}}$  exhibits a very weak dependence on  $\alpha$  and is hardly sensitive to whether the particles are disks or spheres. While in the monocomponent case the degree of rotational-translational nonequipartition is slightly higher in spheres than in disks, from Fig. 5(a) one can observe that this ceases to be true for large enough roughness in the case of mixtures. As for the translational and rotational component-component ratios, the equipartition breakdown is clearly stronger for spheres than for disks, in analogy to what happens in the undriven case (see Fig. 3).

## 5 Mimicry effect

As illustrated by Figs. 3 and 5, in the long-time asymptotic regime each component of a mixture has in general a different translational ( $T_1^{\text{tr}} \neq T_2^{\text{tr}} \neq \dots$ ) and rotational ( $T_1^{\text{rot}} \neq T_2^{\text{rot}} \neq \dots$ ) temperature, both in the driven and the undriven states, even if all the coefficients of restitution and all the reduced moments of inertia are equal ( $\alpha_{ij} = \alpha$ ,  $\beta_{ij} = \beta$ ,  $\kappa_i = \kappa_j = \kappa$ ). An interesting question [29] is whether it is

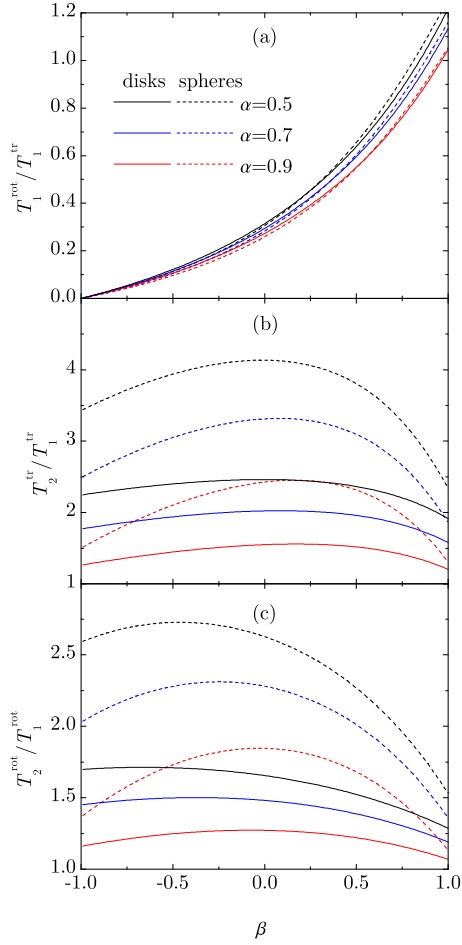


**Fig. 5** Plot of the temperature ratios (a)  $T_1^{\text{rot}}/T_1^{\text{tr}}$ , (b)  $T_2^{\text{tr}}/T_1^{\text{tr}}$ , and (c)  $T_2^{\text{rot}}/T_1^{\text{rot}}$  versus  $\beta$  in systems driven by a stochastic thermostat for equimolar binary mixtures of uniform disks (solid lines) or uniform spheres (dashed lines) with  $\sigma_2/\sigma_1 = 2$ ,  $m_2/m_1 = 2^{d_{\text{tr}}}$ ,  $\beta_{ij} = \beta$ , and  $\alpha_{ij} = \alpha = 0.5$  (black lines),  $0.7$  (blue lines), and  $0.9$  (red lines).

possible to couple the densities, sizes, and masses of the particles in such a way that all the components reach a common translational temperature ( $T_i^{\text{tr}} = T^{\text{tr}}$ ) and a common rotational temperature ( $T_i^{\text{rot}} = T^{\text{rot}}$ ). In that case, the temperature ratio  $T_i^{\text{rot}}/T_i^{\text{tr}} = T^{\text{rot}}/T^{\text{tr}}$  would be the same as that of a monocomponent gas and one can say that the mixture *mimics* the monocomponent system.

Setting  $\alpha_{ij} = \alpha$ ,  $\beta_{ij} = \beta$ ,  $\kappa_i = \kappa_j = \kappa$ ,  $T_i^{\text{tr}} = T^{\text{tr}}$ ,  $T_i^{\text{rot}} = T^{\text{rot}}$ , and  $\mathbf{\Omega}_i = \mathbf{0}$  in Eqs. (2b) and (2c), we obtain

$$\xi_i^{\text{tr,rot}} = \xi_{11}^{\text{tr,rot}} R_i, \quad R_i \equiv \sum_j \frac{n_j \sigma_{ij}^{d_{\text{tr}}-1}}{n_1 \sigma_1^{d_{\text{tr}}-1}} \sqrt{\frac{2m_1 m_j}{m_i(m_i + m_j)}}. \quad (12)$$

According to Eq. (12), the HCS conditions  $\xi_1^{\text{tr}} = \xi_2^{\text{tr}} = \dots = \xi_1^{\text{rot}} = \xi_2^{\text{rot}} = \dots$  decompose into  $\xi_{11}^{\text{tr}} = \xi_{11}^{\text{rot}}$  (which actually is the monocomponent condition) plus  $R_1 = R_2 = \dots$  (which establish constraints on densities, diameters, and masses for the mimicry effect). In the driven case, Eq. (12) shows that  $\xi_i^{\text{rot}} = 0$  implies  $\xi_{11}^{\text{rot}} = 0$  (monocomponent condition), while

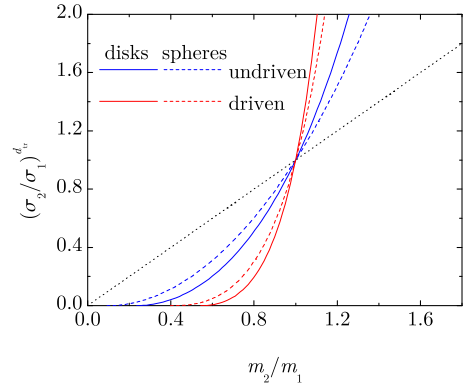


**Fig. 6** Plot of the area or volume ratio  $(\sigma_2/\sigma_1)^{d_{\text{tr}}}$  versus the mass ratio  $m_2/m_1$  for the mimicry effect in equimolar binary mixtures of disks (solid lines) or spheres (dashed lines). The blue and red curves correspond to the undriven and driven systems, respectively. The dotted straight line represents the points  $(\sigma_2/\sigma_1)^{d_{\text{tr}}} = m_2/m_1$  of equal particle mass density.

$\xi_1^{\text{tr}} T_1^{\text{tr}}/m_1 = \xi_2^{\text{tr}} T_2^{\text{tr}}/m_2 = \dots$  imply  $R_1/m_1 = R_2/m_2 = \dots$ . It is remarkable that those mimicry conditions are independent of the coefficients of restitution ( $\alpha$  and  $\beta$ ), the reduced moment of inertia ( $\kappa$ ), and, in the case of the driven system, the noise strength ( $\chi_0^2$ ).

To fix ideas, let us consider a binary mixture. The conditions  $R_1 = R_2$  (undriven system) and  $R_1/m_1 = R_2/m_2$  (driven system) yield

$$\frac{n_2}{n_1} = \frac{\sigma_{12}^{d_{\text{tr}}-1} \varphi(\frac{m_1}{m_2}) \sqrt{\frac{m_1}{m_2}} - \sigma_1^{d_{\text{tr}}-1} \varphi(\frac{m_2}{m_1}) \sqrt{\frac{m_1+m_2}{2m_1}}}{\sigma_{12}^{d_{\text{tr}}-1} \varphi(\frac{m_2}{m_1}) \sqrt{\frac{m_2}{m_1}} - \sigma_2^{d_{\text{tr}}-1} \varphi(\frac{m_1}{m_2}) \sqrt{\frac{m_1+m_2}{2m_2}}}, \quad (13)$$

where  $\varphi(x) = 1$  and  $\varphi(x) = \sqrt{x}$  in the undriven and driven cases, respectively. Equation (13) represents the constraint on  $n_2/n_1$ ,  $\sigma_2/\sigma_1$ , and  $m_2/m_1$  for the mimicry effect. By solving a linear equation in the case of disks ( $d_{\text{tr}} = 2$ ) or a quadratic equation in the case of spheres ( $d_{\text{tr}} = 3$ ), it is possible to express  $\sigma_2/\sigma_1$  as explicit functions of  $n_2/n_1$  and  $m_2/m_1$ . If  $m_2/m_1 \approx 1$ , one has  $\sigma_2/\sigma_1 - 1 = k(m_2/m_1 - 1)/(d_{\text{tr}} - 1)$  with independence of the density ratio, where  $k = \frac{3}{2}$  and  $\frac{7}{2}$  for undriven and driven gases, respectively. It is interesting to notice that the mass ratio  $m_2/m_1$  must be larger than a lower bound (corresponding to  $\sigma_2/\sigma_1 \rightarrow 0$ ) and smaller than an upper bound (corresponding to  $\sigma_2/\sigma_1 \rightarrow \infty$ ). More specifically,  $\mu_0(n_2/n_1) < m_2/m_1 < 1/\mu_0(n_1/n_2)$ , where

$$\mu_0(x) = \frac{x + 2^{d_{\text{tr}}-2} \left[ 2^{d_{\text{tr}}-2} - \sqrt{2^{2(d_{\text{tr}}-2)} + 2(1+x)} \right]}{x^2 - 2^{2d_{\text{tr}}-3}} \quad (14)$$

for undriven gases, while  $\mu_0(x)$  is the positive real root of the quartic equation  $2^{2d_{\text{tr}}-3} \mu_0^3 (1 + \mu_0) = (1 - x \mu_0^2)^2$  for driven gases.

Figure 6 shows the area (in the case of disks) or volume (in the case of spheres) ratio  $(\sigma_2/\sigma_1)^{d_{\text{tr}}}$  as a function of the

mass ratio  $m_2/m_1$ , as obtained from Eq. (13) in the equimolar case ( $n_2/n_1 = 1$ ). If  $m_2 < m_1$ , one has  $(\sigma_2/\sigma_1)^{d_{tr}} < m_2/m_1$ , i.e.,  $m_2/\sigma_2^{d_{tr}} > m_1/\sigma_1^{d_{tr}}$ , while the opposite happens if  $m_2 > m_1$ . Therefore, the mimicry effect requires that the smaller particles have a higher particle mass density than the large spheres, this property holding for any  $n_2/n_1$ . The disparity in the particle mass density is stronger for disks than for spheres and in driven than in undriven systems. In fact, for equimolar mixtures, the windows of mass ratios are  $0.094 < m_2/m_1 < 10.657$ ,  $0.236 < m_2/m_1 < 4.236$ ,  $0.398 < m_2/m_1 < 2.510$ , and  $0.544 < m_2/m_1 < 1.839$  for undriven spheres, undriven disks, driven spheres, and driven disks, respectively.

## 6 Conclusions

In this paper we have carried out a comparative study on the partition of the mean kinetic energy among different classes of degrees of freedom in multicomponent granular gases of disks or spheres. Both undriven (HCS) and driven (stochastic thermostat) states have been considered. The starting point has been a recent unified derivation (within a Maxwellian approximation) of the energy production rates [23] in terms of the number of translational ( $d_{tr}$ ) and rotational ( $d_{rot}$ ) degrees of freedom.

The main conclusions are the following ones: (i) the number of collisions per particle needed to reach stationary values for the temperature ratios is generally smaller for disks than for spheres and in the driven system than in the undriven one; (ii) except in the HCS near the quasi-smooth limit, the relaxation time for the mean angular velocity is much shorter than for the temperature ratios; (iii) while in the driven case the rotational-translational temperature ratio is very similar for disks and spheres, in the undriven case disks typically present a stronger rotational-translational nonequipartition than spheres; (iv) on the other hand, the degree of component-component nonequipartition is higher for spheres than for disks, both for driven and undriven systems; (v) under certain conditions, a multicomponent gas can mimic a monocomponent gas in what concerns the rotational-translational temperature ratio; (vi) this mimicry effect requires the smaller component to have a higher particle mass density than the larger component, this property being more pronounced in the driven system than in the undriven one and for disks than for spheres; (vii) interestingly, a mixture mimicking a monocomponent gas in the undriven state loses its mimicry property in the driven steady state (no matter the intensity of the stochastic force), and vice versa.

**Acknowledgements** The research of A.S. has been supported by the the Agencia Española de Investigación (Spain) through Grant No. FIS2016-76359-P and by the Junta de Extremadura (Spain) through Grant No. GR18079, both partially financed by Fondo Europeo de Desarrollo Regional funds.

## Compliance with ethical standards

*Conflict of interest:* The authors declare that they have no conflict of interest.

## References

- Barrat, A., Trizac, E.: Lack of energy equipartition in homogeneous heated binary granular mixtures. *Granul. Matter* **4**, 57–63 (2002). DOI 10.1007/s10035-002-0108-4
- Behringer, R.P., Chakraborty, B.: The physics of jamming for granular materials: a review. *Rep. Prog. Phys.* **82**, 012601 (2019). DOI 10.1088/1361-6633/aadc3c
- Brilliantov, N.V., Pöschel, T.: *Kinetic Theory of Granular Gases*. Oxford University Press, Oxford (2004)
- Brilliantov, N.V., Pöschel, T., Kranz, W.T., Zippelius, A.: Translations and rotations are correlated in granular gases. *Phys. Rev. Lett.* **98**, 128001 (2007). DOI 10.1103/PhysRevLett.98.128001
- Cornu, F., Piasecki, J.: Granular rough sphere in a low-density thermal bath. *Physica A* **387**, 4856–4862 (2008). DOI 10.1016/j.physa.2008.03.014
- Dahl, S.R., Hrenya, C.M., Garzó, V., Dufty, J.W.: Kinetic temperatures for a granular mixture. *Phys. Rev. E* **66**, 041301 (2002). DOI 10.1103/PhysRevE.66.041301
- Dufty, J.W.: Statistical mechanics, kinetic theory, and hydrodynamics for rapid granular flow. *J. Phys.: Condens. Matter* **12**, A47–A56 (2000). DOI 10.1088/0953-8984/12/8A/306
- Garzó, V., Dufty, J.W.: Homogeneous cooling state for a granular mixture. *Phys. Rev. E* **60**, 5706–5713 (1999). DOI 10.1103/PhysRevE.60.5706
- Garzó, V., Dufty, J.W.: Hydrodynamics for a granular mixture at low density. *Phys. Fluids* **14**, 1476–1490 (2002). DOI 10.1063/1.1458007
- Garzó, V., Dufty, J.W., Hrenya, C.M.: Enskog theory for polydisperse granular mixtures. I. Navier-Stokes order transport. *Phys. Rev. E* **76**, 031303 (2007). DOI 10.1103/PhysRevE.76.031303
- Garzó, V., Montanero, J.M.: Navier–Stokes transport coefficients of  $d$ -dimensional granular binary mixtures at low density. *J. Stat. Phys.* **129**, 27–58 (2007). DOI 10.1007/s10955-007-9357-2
- Garzó, V., Santos, A., Kremer, G.M.: Impact of roughness on the instability of a free-cooling granular gas. *Phys. Rev. E* **97**, 052901 (2018). DOI 10.1103/PhysRevE.97.052901
- Goldhirsch, I.: Rapid granular flows. *Annu. Rev. Fluid Mech.* **35**, 267–293 (2003). DOI 10.1146/annurev.fluid.35.101101.161114
- Goldhirsch, I., Noskovicz, S.H., Bar-Lev, O.: Nearly smooth granular gases. *Phys. Rev. Lett.* **95**, 068002 (2005). DOI 10.1103/PhysRevLett.95.068002
- Huthmann, M., Zippelius, A.: Dynamics of inelastically colliding rough spheres: Relaxation of translational and rotational energy. *Phys. Rev. E* **56**, R6275–R6278 (1997). DOI 10.1103/PhysRevE.56.R6275
- Jenkins, J.T., Mancini, F.: Kinetic theory for binary mixtures of smooth, nearly elastic spheres. *Phys. Fluids A* **1**, 2050–2057 (1989). DOI 10.1063/1.857479
- Jenkins, J.T., Richman, M.W.: Kinetic theory for plane flows of a dense gas of identical, rough, inelastic, circular disks. *Phys. Fluids* **28**, 3485–3494 (1985). DOI 10.1063/1.865302
- Kremer, G.M., Santos, A., Garzó, V.: Transport coefficients of a granular gas of inelastic rough hard spheres. *Phys. Rev. E* **90**, 022205 (2014). DOI 10.1103/PhysRevE.90.022205
- Luding, S.: Granular materials under vibration: Simulations of rotating spheres. *Phys. Rev. E* **52**, 4442–4457 (1995). DOI 10.1103/PhysRevE.52.4442

20. Luding, S., Huthmann, M., McNamara, S., Zippelius, A.: Homogeneous cooling of rough, dissipative particles: Theory and simulations. *Phys. Rev. E* **58**, 3416–3425 (1998). DOI 10.1103/PhysRevE.58.3416
21. Lun, C.K.K., Bent, A.A.: Numerical simulation of inelastic frictional spheres in simple shear flow. *J. Fluid Mech.* **258**, 335–353 (1994). DOI 10.1017/S0022112094003356
22. Lun, C.K.K., Savage, S.B.: A simple kinetic theory for granular flow of rough, inelastic, spherical particles. *J. Appl. Mech.* **54**, 47–53 (1987). DOI 10.1115/1.3172993
23. Megías, A., Santos, A.: Energy production rates of multicomponent granular gases of rough particles. A unified view of hard-disk and hard-sphere systems. arXiv:1809.02327 (2018)
24. Mitarai, N., Hayakawa, H., Nakanishi, H.: Collisional granular flow as a micropolar fluid. *Phys. Rev. Lett.* **88**, 174301 (2002). DOI 10.1103/PhysRevLett.88.174301
25. Montanero, J.M., Garzó, V.: Monte Carlo simulation of the homogeneous cooling state for a granular mixture. *Granul. Matter* **4**, 17–24 (2002). DOI 10.1007/s10035-001-0097-8
26. Montanero, J.M., Santos, A.: Computer simulation of uniformly heated granular fluids. *Granul. Matter* **2**, 53–64 (2000). DOI 10.1007/s100350050035
27. Moon, S.J., Swift, J.B., Swinney, H.L.: Role of friction in pattern formation in oscillated granular layers. *Phys. Rev. E* **69**, 031301 (2004). DOI 10.1103/PhysRevE.69.031301
28. van Noije, T.P.C., Ernst, M.H.: Velocity distributions in homogeneous granular fluids: the free and the heated case. *Granul. Matter* **1**, 57–64 (1998). DOI 10.1007/s100350050009
29. Santos, A.: Interplay between polydispersity, inelasticity, and roughness in the freely cooling regime of hard-disk granular gases. *Phys. Rev. E* **98**, 012804 (2018). DOI 10.1103/PhysRevE.98.012804
30. Santos, A., Kremer, G.M., Garzó, V.: Energy production rates in fluid mixtures of inelastic rough hard spheres. *Prog. Theor. Phys. Suppl.* **184**, 31–48 (2010). DOI 10.1143/PTPS.184.31
31. Santos, A., Kremer, G.M., dos Santos, M.: Sonine approximation for collisional moments of granular gases of inelastic rough spheres. *Phys. Fluids* **23**, 030604 (2011). DOI 10.1063/1.3558876
32. Scholz, C., Pöschel, T.: Velocity distribution of a homogeneously driven two-dimensional granular gas. *Phys. Rev. Lett.* **118**, 198003 (2017). DOI 10.1103/PhysRevLett.118.198003
33. Serero, D., Goldhirsch, I., Noskowicz, S.H., Tan, M.L.: Hydrodynamics of granular gases and granular gas mixtures. *J. Fluid Mech.* **554**, 237–258 (2006). DOI 10.1017/S0022112006009281
34. Uecker, H., Kranz, W.T., Aspelmeier, T., Zippelius, A.: Partitioning of energy in highly polydisperse granular gases. *Phys. Rev. E* **80**, 041303 (2009). DOI 10.1103/PhysRevE.80.041303
35. Vega Reyes, F., Lasanta, A., Santos, A., Garzó, V.: Energy nonequipartition in gas mixtures of inelastic rough hard spheres: The tracer limit. *Phys. Rev. E* **96**, 052901 (2017). DOI 10.1103/PhysRevE.96.052901
36. Vega Reyes, F., Santos, A.: Steady state in a gas of inelastic rough spheres heated by a uniform stochastic force. *Phys. Fluids* **27**, 113301 (2015). DOI 10.1063/1.4934727
37. Vega Reyes, F., Santos, A., Kremer, G.M.: Role of roughness on the hydrodynamic homogeneous base state of inelastic spheres. *Phys. Rev. E* **89**, 020202(R) (2014). DOI 10.1103/PhysRevE.89.020202
38. Williams, D.R.M., MacKintosh, F.C.: Driven granular media in one dimension: Correlations and equation of state. *Phys. Rev. E* **54**, R9–R12 (1996). DOI 10.1103/PhysRevE.54.R9
39. Zamankhan, P., Tafreshi, H.V., Polashenski, W., Sarkomaa, P., Hyndman, C.L.: Shear induced diffusive mixing in simulations of dense Couette flow of rough, inelastic hard spheres. *J. Chem. Phys.* **109**, 4487–4491 (1998). DOI 10.1063/1.477076